Materials Research
Express

PAPER • OPEN ACCESS

Thermoelectric performance enhancement of Mg_2Si-based silicides synthesized in nitrogen atmosphere

To cite this article: Samantha Faye Duran Solco *et al* 2024 *Mater. Res. Express* **11** 125505

IOP Publishing | Mater. Res. Express 11 (2024) 125505 | https://doi.org/10.1088/2053-1591/ad9cf1

Materials Research Express

CrossMark

OPEN ACCESS

RECEIVED
23 August 2024

REVISED
2 December 2024

ACCEPTED FOR PUBLICATION
10 December 2024

PUBLISHED
20 December 2024

PAPER

Thermoelectric performance enhancement of Mg_2Si-based silicides synthesized in nitrogen atmosphere

Samantha Faye Duran Solco[1], Kivanc Saglik[1,2], Danwei Zhang[1], Xian Yi Tan[1], Qiang Zhu[1,3], Hongfei Liu[1], Ady Suwardi[4,*] and Jing Cao[1,5,*]

[1] Institute of Materials Research and Engineering, Agency for Science, Technology and Research, 138634, Singapore
[2] School of Materials Science and Engineering, Nanyang Technological University, 639798, Singapore
[3] School of Chemistry, Chemical Engineering and Biotechnology, Nanyang Technological University, 637371, Singapore
[4] Department of Electronic Engineering and Shun Hing Institute of Advanced Engineering, The Chinese University of Hong Kong, Sha Tin, New Territories, 999077, Hong Kong
[5] Department of Materials Science and Engineering, National University of Singapore, 117575, Singapore
[*] Authors to whom any correspondence should be addressed.

E-mail: asuwardi@ee.cuhk.edu.hk **and** cao_jing@imre.a-star.edu.sg

Keywords: thermoelectricity, energy harvesting, sustainability, silicides, thermal transport

Supplementary material for this article is available online

Abstract

In this work, we compare the thermoelectric performance of Mg_2Si-based compounds by synthesizing them in N_2 compared to Ar atmosphere during ball milling. In addition, we achieved high thermoelectric performance by introducing Sn-alloying as well as Zn- and Bi-co doping. The high performance originated from simultaneous improvement in electrical conductivity and reduced thermal conductivity. This results in peak zT near 1.0 at 760 K for $Mg_{1.9925}Zn_{0.0075}Si_{0.48}Sn_{0.5}Bi_{0.02}$. Owing to the much lower cost (higher abundance) of N_2 compared to Ar owing to their much higher relative abundance, such processing strategy is expected to improve sustainability. Furthermore, the insights derived from this work can potentially be applied to other compounds containing Mg- and other reactive elements. Fundamentally, this result will also motivate further studies on the intrinsic defect formation in N_2 vs Ar atmosphere, which affects both electronic and thermal transports.

1. Introduction

Rapidly changing climate, driven by overconsumption of energy and electricity has imposed pressing needs to innovate sustainable materials for renewable energy needs. Amongst other renewable energy technologies, thermoelectrics, with their special ability to inter-convert heat and electricity have a special role to play. For instance, their ability to upcycle waste heat into electricity makes them attractive to augment other technologies such as photovoltaics to capture the portion of energy that would otherwise be wasted as waste heat. On the other hand, the ability of thermoelectrics to function as solid-state cooler is valuable for cooling down heat-sensitive components among existing technologies such as batteries and modern electronics. Yet, despite their tremendous potential, the widespread adoption of thermoelectrics is generally limited by both their performance and overall cost [1–4].

In terms of performance, a thermoelectric material is generally defined by both electronic and thermal transport parameters, which makes up the figure-of-merit $zT = S^2\sigma T/\kappa$, with S, σ, and κ denoting Seebeck coefficient, electrical, and thermal conductivity, respectively. To achieve high zT, multiple strategies such as engineering scattering mechanisms, interstitial doping, band convergence, and nanostructuring are commonly used [5–8]. In addition, various types of defects, lattice anharmonicity, complex structures, hierarchical structure, and lattice strain have been popularly used to reduce lattice thermal conductivity [9–15]. In recent years, several key materials have emerged to be the leading performer amongst thermoelectrics such as GeTe, SnSe, Cu_2Se, Mg_3Sb_2, and $AgSbTe_2$ based compounds [6, 16–33]. For designing high performance materials, besides materials selection, the processing parameters are often deterministic. For instance, majority of thermoelectric materials synthesis are done in vacuum to prevent oxidation, which is very detrimental to their performance. This has also posed great challenges in device fabrication and additive manufacturing for thermoelectrics, especially for thin films, as laid out by Tan, *et al* [2, 34–41]. Furthermore, for compounds containing highly reactive and volatile elements such as Mg, inert gas such as Ar is popularly used to prevent unwanted reaction. As such, due to the stringent requirements during synthesis and processing, lack of upcycling efforts, and not to mention tedious device fabrication, the overall cost of thermoelectric devices are often forbiddingly high [42–46]. This often renders it uneconomical to use thermoelectric for large scale energy harvesting applications.

One good example of Mg-containing compound with good thermoelectric performance is magnesium silicide (Mg_2Si). It is a narrow bandgap *n*-type semiconductor with high electrical conductivity and low thermal conductivity, nontoxic, pollution-free, and corrosion-resistant [47]. Mg_2Si is a well-studied compound, with high thermoelectric performance previously using various doping/alloying strategies using Sn alloying or doping with Bi, Sb, Zn, Ga, Pb, Sr, and Al [48–58]. In terms of synthesis, various methods ranging induction melting, vertical Bridgman growth, spark plasma sintering, solid state reaction and microwave have been explored [50, 59–63]. Many of these processes involve pulverizing the ingot of the Mg_2Si sample in Ar-protected atmosphere. Therefore, barring its stringent requirement of Ar-protected atmosphere, it is an otherwise environmentally friendly and economical medium-temperature thermoelectric material with high power conversion efficiency [64, 65].

Motivated by the importance of exploring greener and cheaper processing, in this work, we explore the processing of Mg_2Si using N_2 compared to Ar. N_2 is a greener and cheaper alternative to Ar owing to its higher relative abundance. In terms of abundance, N_2 and Ar make up of 78% and 0.93% of air-content, respectively. In terms of cost, Ar is three times more expensive than N_2. The synthesis of Mg_2Si and Mg_2Ge in N_2 atmosphere using a microwave-induced-metal-plasma method has been performed by Fan *et al*, which demonstrates the possibility of utilizing N_2 gloveboxes in the formation of Mg-based compounds [49]. While the work mentions thermoelectricity as a potential application of Mg_2Si, further experimentation and testing of the electrical and thermal transport properties are required to analyze if this synthesis method is suitable for thermoelectric materials. It is evident from our study that while both N_2 and Ar result in pure phase Mg_2Si, the sample synthesized in N_2 atmosphere has simultaneously higher electrical conductivity and lower thermal conductivity. As a result, high zT of close to 0.5 at 760 K was achieved, which is among one of the highest performance of undoped Mg_2Si in the literatures. To demonstrate performance closer to the state-of-art value of optimized Mg_2Si-based compounds, further alloying with Sn and co-doping with Zn and Bi results in zT close to 1.0 at 760 K, competitive with other $Mg_2Si_{1\text{-}x}Sn_x$ performances [66]. The strategy and insights in this work can be envisaged for other Mg-based materials such as the Mg_3Sb_2, which is a promising alternative for Bi_2Te_3-based compounds for room temperature applications. More importantly, in terms of the fundamental of intrinsic defects, this work can spur on further studies in understanding the role of N_2 in modulating the defect formation within Mg_2Si, which was traditionally understood to be originated from the concentration of electrons in the tiny cavity spaces formed by Mg-sublattice [67].

2. Methods

High purity (>99.999%) Si chunks, Mg chunks from ZhongNuo Advanced Material Technology Co. Ltd were weighed in stoichiometric ratios under N_2-protected or Ar-protected atmosphere with 10% excess of Mg to compensate for the loss of this element during ball milling. The mixture was ball milled in sealed tungsten carbide (WC) jars for 2 h, in which stearic acid was added in WC jars to prevent the adhesion of the bulk material to the jar. Then the mixture powders were heated in the glovebox to 400 °C to remove the stearic acid, and cold-pressed (in vacuum of 1.0 Pa) into pellets under a pressure of 7 MPa for 2 min with the diameter of 13 mm. The Self-propagating high-temperature synthesis (SHS) process was firstly started by vacuum sealing the pressed pellets at a pressure of 10^{-3} Pa in quartz ampules to prevent any oxygen from reacting with sample before SHS, then heating the bottom of the pellets in vacuum with a hand torch. Once ignited, the hand torch is removed immediately. Then the pellets were grounded into fine powders carefully by hand in N_2-protected or Ar-protected atmosphere, then the fine powders were detected by XRD to determine whether magnesium silicide is pure. Spark Plasma Sintering (SPS) at 1073 K and 1 pa vacuum, under a pressure of 50 MPa for 10 min was utilized to densify the homogenized powder. The size of the graphite die was 12.7 mm in diameter. After which, the final sintered pellets were cut and polished to test for electronic and thermal properties.

For the thermoelectric properties, electrical resistivity and Seebeck coefficient were measured simultaneously using ZEM-3 from ULVAC. The thermal properties were measured using laser LFA 457, NETZSCH. The heat capacity used for thermal conductivity calculation was estimated using Dulong-Petit

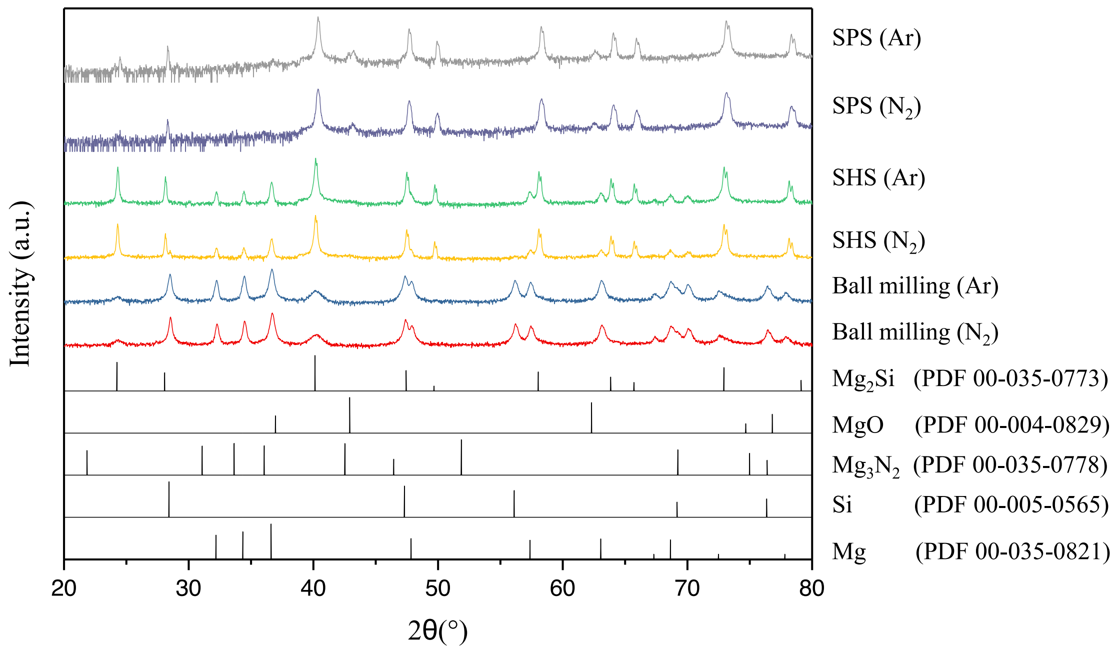

Figure 1. XRD scans of Mg_2Si after ball milling, SHS and on final pellet after SPS.

approximation, with correction term to account for thermal expansion [68]. XRD characterization was conducted at room temperature. Microscopy analysis was done in field emission scanning electron microscopy.

3. Results and discussion

In order to ascertain the percentage of Mg in different stages, X-ray diffraction (XRD) was done after ball milling, SHS and on the final sample, as shown in figure 1. It is worth noting that after 2 h ball milling, the powders consist mostly of Mg and Si, some Mg_2Si is detectable. This stems from incomplete reaction between Mg and Si. Subsequently, after SHS, most of the product is Mg_2Si, with minor residual Mg peaks, presumably due to the excess Mg introduced during synthesis. Lastly, after the SPS, the minor peaks belonging to Mg disappear due to its volatility, with the resulting product purely Mg_2Si. The characteristic peaks are indicative of a highly crystalline material and matched well with the indexed pristine Mg_2Si [69], which can be observed at around 40°. Furthermore, for sample synthesized with SHS in N_2, no oxide phase can be observed from the figure, which suggests that minimal oxidation occur during the synthesis and consolidation processes. This is in contrast to the same sample synthesized using SPS method in N_2, which shows minor peaks of MgO. This observation is important since the presence of oxide phase has been known to be detrimental to the electronic transport properties. In addition, the resulting sample appears homogeneous with no observable agglomeration or phase separation under electron microscopy, as shown in figure S1. Importantly, no structural difference can be observed between sample synthesized in N_2 and Ar atmosphere.

To further elucidate the thermoelectric properties, both the electronic transport consisting of Seebeck coefficient (S) and electrical conductivity (σ) and thermal transport (κ) were measured, as shown in figure 2. Evidently, the value of Seebeck coefficient, electrical conductivity and power factor for Mg_2Si (N_2) is higher than in Mg_2Si (Ar), as shown in figures 2(a)–(c). Figure 2(a) shows a general trend of decreasing electrical conductivity across the entire temperature range, consistent with degenerate behavior and also with increasing magnitude of Seebeck shown in figure 2(b). The origin of the higher electrical conductivity of sample synthesized in N_2 atmosphere can possibly come from the presence of Mg in interstitial sites [70]. This can be associated with the starting composition of 10% excess Mg, which might have over compensated for Mg loss during synthesis. In addition, in comparison to literatures, samples synthesized using the combination of SHS and SPS generally show higher electrical conductivity and power factor compared to other synthesis routes, as demonstrated by the current work and the work by Zhang, *et al.* which also employed SHS and SPS in their synthesis [71].

In terms of thermal transport, despite having higher electrical conductivity, Mg_2Si (N_2) also has lower thermal conductivity compared to Mg_2Si (Ar), as shown in figure 2(d). As a result, the estimated lattice thermal conductivity of Mg_2Si (N_2) is drastically lower compared to Mg_2Si (Ar) in figure 2(e). Interestingly, the results from Tani, *et al* and Cederkrantz, *et al* also shows lower lattice thermal conductivity as compared to Mg_2Si (Ar)

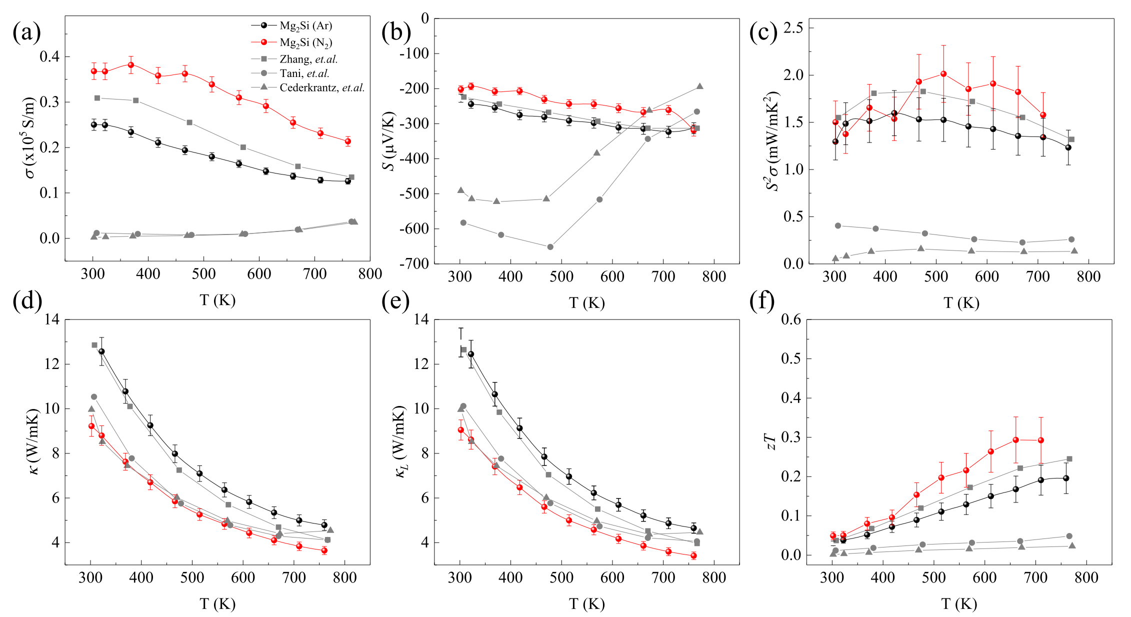

Figure 2. Thermoelectric properties of Mg_2Si synthesized in Ar, N_2, compared to Mg_2Si from literatures [53, 71, 72]. (a) Electrical conductivity (b) Seebeck coefficient (c) Power factor (d) Thermal conductivity (e) Lattice thermal conductivity, and (f) zT as the function of temperatures.

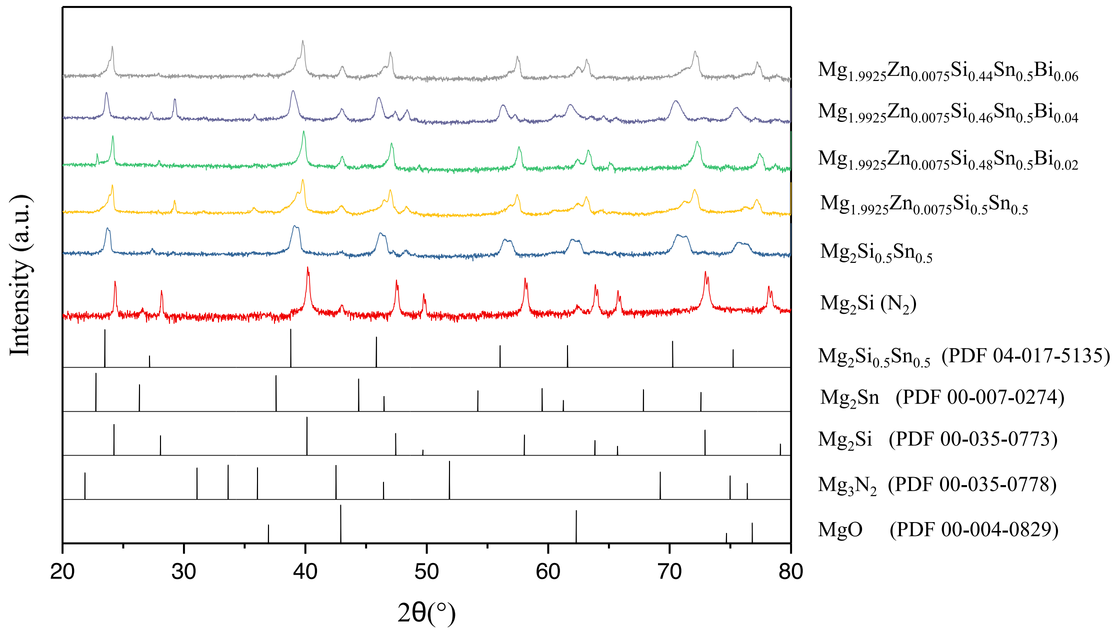

Figure 3. XRD scans of Mg_2Si alloyed with Sn and co-doped with Zn and Bi after SPS.

and result from Zhang, *et al* [53, 71, 72]. This can be associated with difference in processing conditions. In the reports by Tani, *et al* and Cederkrantz, *et al*, the samples were prepared by direct SPS and ball milling followed by SPS, respectively. Trace amount of unreacted silicon and magnesium may have contributed to nanoprecipitate phonon scattering in the samples by Tani, *et al* and Cederkrantz, *et al* On the other hand, the possible presence of Mg_3N_2 in Mg_2Si (N_2) may have resulted in increased phonon scattering and thus lower lattice thermal conductivity. Consequently, reasonably high zT value near 0.5 at 760 K was achieved in Mg_2Si (N_2), as shown in figure 2(f). This is among the highest value compared to undoped Mg_2Si in the literatures so far.

To demonstrate the feasibility of further alloying and doping to enhance the zT of Mg_2Si (N_2), Sn alloying as well as Zn- and Bi- co-doping were introduced to the samples. As evident from figure 3, the alloying of Sn into $Mg_2Sn_{0.5}Si_{0.5}$ shifted the peaks to lower angles. This is due to the larger ionic radii of Sn^{4+} compared to Si^{4+}, which results in higher lattice parameters, as shown in figure S2. On the other hand, introduction of Zn into Mg

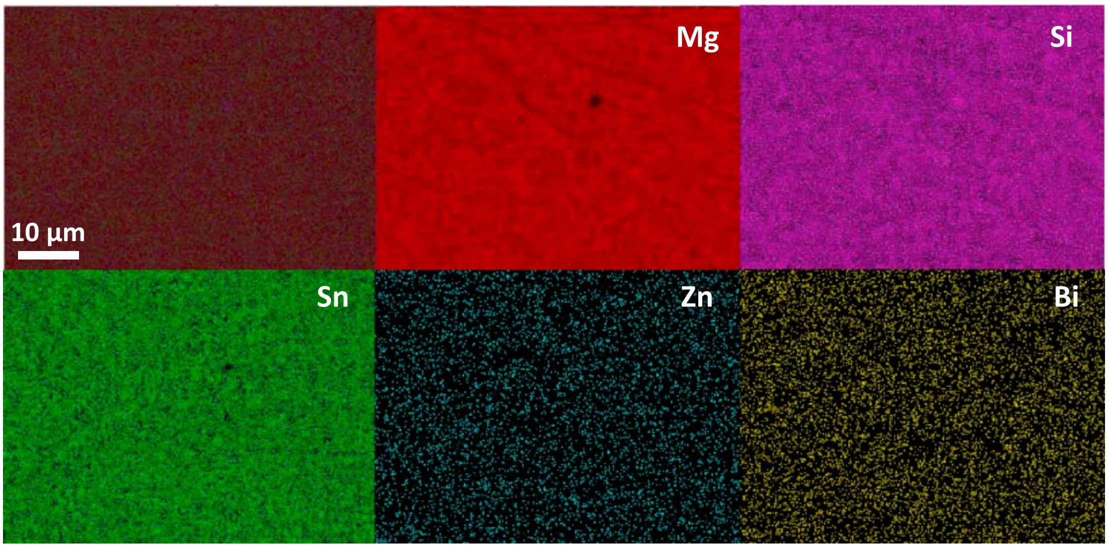

Figure 4. EDS scans of $Mg_{1.9925}Zn_{0.0075}Si_{0.48}Sn_{0.5}Bi_{0.02}$.

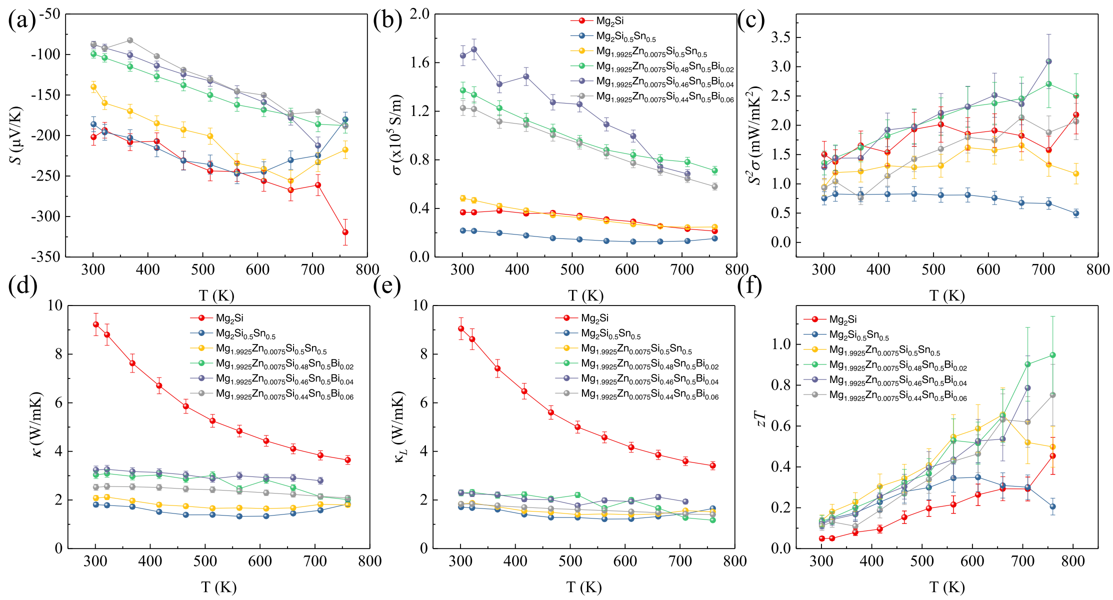

Figure 5. Thermoelectric properties of Zn and Bi doped $Mg_2Si_{0.5}Sn_{0.5}$ (a) Seebeck coefficient (b) Electrical conductivity (c) Power factor (d) Thermal conductivity (e) Lattice thermal conductivity, and (f) zT as the function of temperatures.

sites reduced the lattice parameter due to the slightly smaller ionic radii of Zn^{2+} than Mg^{2+}. Lastly, doping Bi into the Si/Sn sites gradually increases the lattice parameter due to the large ionic radii of Bi. It is noteworthy that in all samples, no obvious secondary phase peaks can be observed.

To ascertain the homogeneous distribution of the Sn, Zn, and Bi dopants in the samples, EDS was done on $Mg_2Si_{0.5}Sn_{0.5}$ and $Mg_{1.9925}Zn_{0.0075}Si_{0.48}Sn_{0.5}Bi_{0.02}$, as shown in figure S3 and figure 4, respectively. Besides the minute precipitates of elemental Si in both samples, the rest of the areas are quite homogeneously distributed. Importantly, although there appears to be peak broadening in $Mg_2Si_{0.5}Sn_{0.5}$ in figure 3, the EDS in figure S3 does not show any large area agglomeration of secondary phase. In addition, the quantitative analysis in table S1 shows that the weight percentage of the elements are commensurate with the sample composition.

In terms of thermoelectric properties, the alloying of Sn into Mg_2Si does not significantly alter the Seebeck coefficient at low temperatures, as shown in figure 5(a). Interestingly, at above 600 K, the magnitude of Seebeck coefficient of $Mg_2Si_{0.5}Sn_{0.5}$ increases with temperature, which deviates from the trend for Mg_2Si. This can be explained by the reduced band-gap upon alloying with Sn, which results in onset of bipolar conduction at lower temperatures [66]. In addition, the lower electrical conductivity of $Mg_2Si_{0.5}Sn_{0.5}$ can be attributed to the alloy scattering brought about by Sn atoms, which reduced the carrier mobility in the sample (figure 5(b)). Besides alloying with Sn, minute doping of Zn and Bi results in drastically enhanced electrical conductivity, which also results in increased power factor compared to pristine Mg_2Si (figure 5(c)). Notably, the bipolar onset of $Mg_2Si_{0.5}Sn_{0.5}$ is suppressed upon introduction of Zn and Bi. This can be attributed to the role of higher carrier concentration in suppressing bipolar effects. As a result, considerably higher power factor can be achieved at higher temperatures ($>$ 700 K) for all Zn and Bi doped samples.

In terms of thermal transport properties, the introduction of Sn alloying drastically reduce both total thermal conductivity and lattice thermal conductivity. This is due to the combination of alloy scattering and higher anharmonicity due to larger atomic mass of Sn compared to Si [73, 74]. It is noteworthy that further addition of minute Zn and Bi does not alter the lattice thermal conductivity appreciably. Consequently, high peak zT can be achieved for all $Mg_2Si_{0.5}Sn_{0.5}$-based samples doped with Zn and Bi primarily due to their higher power factor. It has to be noted that due to Mg-loss at high temperatures, performance degradation may occur. This was well examined in previous study by Sankhla *et al* [75].

4. Conclusions

In this work, N_2 was explored as the alternative protective gas for the processing of Mg_2Si due to its higher relative abundance compared to Ar. While XRD results do not show any difference between N_2 and Ar synthesized sample, their transport properties differ quite drastically from each other. The sample synthesized in N_2 atmosphere has simultaneously higher electrical conductivity and lower thermal conductivity than the one synthesized in Ar atmosphere. This results in high zT of close to 0.5 at 760 K, which is the highest performance of undoped Mg_2Si compared to the literatures. Furthermore, alloying with Sn and co-doping with Zn and Bi results in zT close to 1.0 at 760 K, which is competitive to the performance of other $Mg_2Si_{1\text{-}x}Sn_x$ mainly synthesized in Ar protected atmosphere. Overall, the strategy of replacing Ar with N_2 in this work can be envisaged for other compounds with reactive and volatile elements. It is worth mentioning that this work leaves further scope for exploration in terms of understanding the effect of N_2 on the intrinsic defect formation mechanisms, which ultimately determines the electronic and thermal transport properties.

Acknowledgments

This research is supported in part by project #RNE-p3-24 of the Shun Hing Institute of Advanced Engineering, The Chinese University of Hong Kong. A.S. also acknowledges funding from CUHK Direct Grant 4055224, and startup funding from The Chinese University of Hong Kong. J.C. acknowledges funding from e-Asia Joint Research Program award no. R22I1IR053, and LCER Phase 2 ETGC award no. U2411D4011.

Data availability statement

All data that support the findings of this study are included within the article (and any supplementary files).

Supporting information

Additional experimental details, performance repeatability data, compositional, and transport data are available can be found in Supporting Information.

Declaration

The authors declare no competing financial interest.

Author contributions

The manuscript was written through contributions of all authors. All authors have given approval to the final version of the manuscript.

ORCID iDs

Samantha Faye Duran Solco https://orcid.org/0000-0002-6335-9972
Hongfei Liu https://orcid.org/0000-0002-9905-7028
Ady Suwardi https://orcid.org/0000-0002-7342-0431
Jing Cao https://orcid.org/0000-0002-7853-573X

References

[1] Jia N, Cao J, Tan X Y, Dong J, Liu H, Tan C K I, Xu J, Yan Q, Loh X J and Suwardi A 2021 Thermoelectric materials and transport physics *Mater. Today Phys.* **21** 100519
[2] Cao J, Tan X Y, Dong J, Liu H, Zheng Y, Zhu Q, Xu J, Zhang G, Wu J and Suwardi A 2023 Thermoelectric device performance beyond average ZT: Holistic consideration of materials and design *Mater. Today Phys.* **34** 101071
[3] Dong J, Suwardi A, Tan X Y, Jia N, Saglik K, Ji R, Wang X, Zhu Q, Xu J and Yan Q 2023 Challenges and opportunities in low-dimensional thermoelectric nanomaterials *Mater. Today* (https://doi.org/10.1016/j.mattod.2023.04.021)
[4] Yang S, Qiu P, Chen L and Shi X 2021 Recent developments in flexible thermoelectric devices *Small Science.* **1** 2100005
[5] Ng H K, Xiang D, Suwardi A, Hu G, Yang K, Zhao Y, Liu T, Cao Z, Liu H and Li S 2022 Improving carrier mobility in two-dimensional semiconductors with rippled materials *Nat. Electron.* **5** 489–96
[6] Cao J, Tan X Y, Jia N, Lan D, Solco S F D, Chen K, Chien S W, Liu H, Tan C K I and Zhu Q 2022 Improved zT in Nb 5 Ge 3–GeTe thermoelectric nanocomposite *Nanoscale.* **14** 410–8
[7] Liu F, Zhang M, Nan P, Zheng X, Li Y, Wu K, Han Z, Ge B, Zhao X and Fu C 2023 Unraveling the origin of donor-like effect in bismuth–telluride-based thermoelectric materials *Small Science.* 2300082
[8] Chen R, Yan Y, Tang J, Zeng H, Yao Q, Chen L and Liang Z 2022 Efficient p-Type doping of tin halide perovskite via sequential diffusion for thermoelectrics *Small Science.* **2** 2200004
[9] Zhu B, Su X, Shu S, Luo Y, Tan X Y, Sun J, Sun D, Zhang H, Zhang Q and Suwardi A 2022 Cold-sintered Bi_2Te_3-based materials for engineering nanograined thermoelectrics *ACS Appl. Energy Mater.* **5** 2002–10
[10] Bauer C, Veremchuk I, Kunze C, Benad A, Dzhagan V M, Haubold D, Pohl D, Schierning G, Nielsch K and Lesnyak V 2021 Heterostructured bismuth telluride selenide nanosheets for enhanced thermoelectric performance *Small Science* **1** 2000021
[11] Yang X, Yuan S, Guo K, Ni H, Song T, Lyu W, Wang D, Li H, Pan S and Zhang J 2022 Achieving low lattice thermal conductivity in half-heusler compound LiCdSb via zintl chemistry *Small Science.* **2** 2200065
[12] Ong P J, Png Z M, Soo X Y D, Wang X, Suwardi A, Chua M H, Xu J W and Zhu Q 2022 Surface modification of microencapsulated phase change materials with nanostructures for enhancement of their thermal conductivity *Mater. Chem. Phys.* **277** 125438
[13] Wang D Z, Liu W D, Li M, Zheng K, Hu H, Yin L C, Wang Y, Zhu H, Shi X L and Yang X 2023 Hierarchical architectural structures induce high performance in n-Type GeTe-based thermoelectrics. *Adv. Funct. Mater.* **33** 2213040
[14] Suwardi A, Prasad B, Lee S, Choi E-M, Lu P, Zhang W, Li L, Blamire M, Jia Q and Wang H 2016 Turning antiferromagnetic Sm 0.34 Sr 0.66 MnO 3 into a 140 K ferromagnet using a nanocomposite strain tuning approach *Nanoscale* **8** 8083–90
[15] Cao J, Zheng J, Liu H, Tan C K I, Wang X, Wang W, Zhu Q, Li Z, Zhang G and Wu J 2022 Flexible elemental thermoelectrics with ultra-high power density *Materials Today Energy.* **25** 100964
[16] Cao J, Chien S W, Tan X Y, Tan C K I, Zhu Q, Wu J, Wang X, Zhao Y, Yang L and Yan Q 2021 Realizing zT values of 2.0 in cubic GeTe *Chem Nano Mat* **7** 476–82
[17] Zheng Y, Xie H, Zhang Q, Suwardi A, Cheng X, Zhang Y, Shu W, Wan X, Yang Z and Liu Z 2020 Unraveling the critical role of melt-spinning atmosphere in enhancing the thermoelectric performance of p-type Bi0. 52Sb1. 48Te3 alloys *ACS Appl. Mater. Interfaces* **12** 36186–95
[18] Zhu B, Luo Y, Wu H, Sun D, Liu L, Shu S, Luo Z-Z, Zhang Q, Suwardi A and Zheng Y 2023 Enhanced thermoelectric performance in Bi 0.5 Sb 1.5 Te 3/SiC composites prepared by low-temperature liquid phase sintering *J. Mater. Chem.* A **11** 8912–21
[19] Cao J, Tan X Y, Jia N, Zheng J, Chien S W, Ng H K, Tan C K I, Liu H, Zhu Q and Wang S 2022 Designing good compatibility factor in segmented Bi0. 5Sb1. 5Te3–GeTe thermoelectrics for high power conversion efficiency *Nano Energy.* **96** 107147
[20] Cao J, Dong J, Saglik K, Zhang D, Solco S F D, You I J W J, Liu H, Zhu Q, Xu J and Wu J 2023 Non-equilibrium strategy for enhancing thermoelectric properties and improving stability of $AgSbTe_2$ *Nano Energy.* **107** 108118
[21] Roychowdhury S, Ghosh T, Arora R, Samanta M, Xie L, Singh N K, Soni A, He J, Waghmare U V and Biswas K 2021 Enhanced atomic ordering leads to high thermoelectric performance in $AgSbTe_2$ *Science* **371** 722–7
[22] Dong J, Jiang Y, Liu J, Pei J, Tan X Y, Hu H, Suwardi A, Jia N, Liu C and Zhu Q 2022 High thermoelectric performance in GeTe with compositional insensitivity *Nano Energy.* **103** 107809
[23] Wang X, He H, Yin L, Cheng J, Sui J, Liu X, Mao J, Cao F and Zhang Q 2022 Infinite coordination polymer for enhancing the thermoelectric performance of Bi0. 5Sb1. 5Te3 for low-grade waste heat recovery *Materials Today Energy.* **26** 100994
[24] Norifusa S, Masaji O, Jin K and Takao M 2022 A hierarchical design for thermoelectric hybrid materials: Bi_2Te_3 particles covered by partial Au skins enhance thermoelectric performance in sticky thermoelectric materials *A Hierarchical Design For Thermoelectric Hybrid Materials: Bi_2te_3 Particles Covered By Partial Au Skins Enhance Thermoelectric Performance In Sticky Thermoelectric Materials* **2** 15
[25] Zhang Z, Zhao K, Wei T-R, Qiu P, Chen L and Shi X 2020 Cu 2 Se-Based liquid-like thermoelectric materials: Looking back and stepping forward *Energy Environ. Sci.* **13** 3307–29
[26] Liu D, Wang D, Hong T, Wang Z, Wang Y, Qin Y, Su L, Yang T, Gao X and Ge Z 2023 Lattice plainification advances highly effective SnSe crystalline thermoelectrics *Science* **380** 841–6
[27] Suwardi A, Cao J, Zhao Y, Wu J, Chien S W, Tan X Y, Hu L, Wang X, Wang W and Li D 2020 Achieving high thermoelectric quality factor toward high figure of merit in GeTe *Mater. Today Phys.* **14** 100239
[28] Suwardi A, Cao J, Hu L, Wei F, Wu J, Zhao Y, Lim S H, Yang L, Tan X Y and Chien S W 2020 Tailoring the phase transition temperature to achieve high-performance cubic GeTe-based thermoelectrics *J. Mater. Chem.* A **8** 18880–90
[29] Suwardi A, Lim S H, Zheng Y, Wang X, Chien S W, Tan X Y, Zhu Q, Wong L M N, Cao J and Wang W 2020 Effective enhancement of thermoelectric and mechanical properties of germanium telluride via rhenium-doping *J. Mater. Chem.* C **8** 16940–8
[30] Jiang B *et al* 2021 High-entropy-stabilized chalcogenides with high thermoelectric performance *Science* **371** 830–4
[31] Mao J, Zhu H, Ding Z, Liu Z, Gamage G A, Chen G and Ren Z 2019 High thermoelectric cooling performance of n-type Mg_3Bi_2-based materials *Science* **365** 495–8

[32] Tsuda S, Yoshinari A, Takezawa S, Ohishi K, Nagamura N, Zhang W, Iwasaki Y and Takagiwa Y 2023 Effect of carrier doping on the electronic states of earth-abundant Fe-Al-Si thermoelectric materials *Mater. Res. Express* **10** 055506
[33] Meena D K, Bose R S, Umarji A and Babu D A 2023 Polymer-mixed Sb2Te3/Te nanocomposites exhibiting p-type to n-type conduction reversal and thermal conductivity reduction *Mater. Res. Express* **10** 074001
[34] Tan M, Liu W-D, Shi X-L, Sun Q and Chen Z-G 2023 Minimization of the electrical contact resistance in thin-film thermoelectric device *Appl. Phys. Rev.* **10**
[35] Zhang D, Lim W Y S, Duran S S F, Loh X J and Suwardi A 2022 Additive manufacturing of thermoelectrics: emerging trends and outlook *ACS Energy Lett.* **7** 720–35
[36] Zhang D, Lim X J G, Li X, Saglik K, Solco S F D, Tan X Y, Leow Y, Zhai W, Tan C K I and Xu J 2022 3D-Printed porous thermoelectrics for in situ energy harvesting *ACS Energy Lett.* **8** 332–8
[37] Danwei Z, Seng Ann S, Samantha Faye Duran S, Jianwei X and Ady S 2023 Energy harvesting through thermoelectrics: topological designs and materials jetting technology *Energy Harvesting Through Thermoelectrics: Topological Designs And Materials Jetting Technology* **3** 1
[38] Tan L P, Sun T, Fan S, Ng L Y, Suwardi A, Yan Q and Hng H H 2013 Facile synthesis of Cu7Te4 nanorods and the enhanced thermoelectric properties of Cu7Te4–Bi0. 4Sb1. 6Te3 nanocomposites *Nano Energy* **2** 4–11
[39] Suwardi A, Hu L, Wang X, Tan X Y, Repaka D V M, Wong L-M, Ni X, Liew W H, Lim S H and Yan Q 2020 Origin of high thermoelectric performance in earth-abundant phosphide–tetrahedrite. *ACS Appl. Mater. Interfaces* **12** 9150–7
[40] Zhang D, Ramiah J, Cagirici M, Saglik K, Solco S F D, Cao J, Xu J and Suwardi A 2024 Thermoelectric nanowires for dense 3D printed architectures *Materials Horizons.* **11** 847–54
[41] Zhang D, Ngoh Yen Qi N, Faye Duran Solco S, Li X and Suwardi A 2024 Lattice architectures for thermoelectric energy harvesting *ACS Energy Lett.* **9** 2240–7
[42] Liu H, Tan C K I, Meng T L, Lin M, Lee C J, Liu J, Zhang Z, Tan D C, Cao J and Suwardi A 2022 Direct deposition of low-cost carbon fiber reinforced stainless steel composites by twin-wire arc spray *J. Mater. Process. Technol.* **301** 117440
[43] Zheng J, Solco S F D, Wong C J E, Sia S A, Tan X Y, Cao J, Yeo J C C, Yan W, Zhu Q and Yan Q 2022 Integrating recyclable polymers into thermoelectric devices for green electronics *J. Mater. Chem.* A **10** 19787–96
[44] Yazawa K and Shakouri A 2011 Cost-efficiency trade-off and the design of thermoelectric power generators *Environmental Science & Technology* **45** 7548–53
[45] Yee S K, LeBlanc S, Goodson K E and Dames C 2013 $ per W metrics for thermoelectric power generation: beyond ZT *Energy Environ. Sci.* **6** 2561–71
[46] Zhang D, Xie M, Safanama D, Saglik K, Tan X Y, Solco S F D, Cao J, Tan C K I, Liu H and Wang S 2023 Sb Alloying for engineering high-thermoelectric zT of CuGaTe2 *Advanced Energy and Sustainability Research.* 2300069
[47] Hirayama N, Iida T, Sakamoto M, Nishio K and Hamada N 2019 Substitutional and interstitial impurity p-type doping of thermoelectric Mg2Si: a theoretical study *Sci. Technol. Adv. Mater.* **20** 160–72
[48] Satyala N and Vashaee D 2012 Modeling of thermoelectric properties of magnesium silicide (Mg 2 Si) *J. Electron. Mater.* **41** 1785–91
[49] Ihou-Mouko H, Mercier C, Tobola J, Pont G and Scherrer H 2011 Thermoelectric properties and electronic structure of p-type Mg2Si and Mg2Si0. 6Ge0. 4 compounds doped with Ga *J. Alloys Compd.* **509** 6503–8
[50] Fiameni S, Battiston S, Boldrini S, Famengo A, Agresti F, Barison S and Fabrizio M 2012 Synthesis and characterization of Bi-doped Mg2Si thermoelectric materials *J. Solid State Chem.* **193** 142–6
[51] Li G, He J, An Q, Morozov S I, Hao S, Zhai P, Zhang Q, Goddard W A III, Snyder and G J 2019 Dramatically reduced lattice thermal conductivity of Mg2Si thermoelectric material from nanotwinning *Acta Mater.* **169** 9–14
[52] Battiston S, Fiameni S, Saleemi M, Boldrini S, Famengo A, Agresti F, Stingaciu M, Toprak M S, Fabrizio M and Barison S 2013 Synthesis and characterization of Al-doped Mg 2 Si thermoelectric materials *J. Electron. Mater.* **42** 1956–9
[53] Tani J-i and Kido H 2007 Thermoelectric properties of Sb-doped Mg2Si semiconductors *Intermetallics* **15** 1202–7
[54] Kaur K, Dhiman S and Kumar R 2017 Strain engineering on thermoelectric performance of Mg2Si *Mater. Res. Express* **4** 075509
[55] Fan T, Xie C, Wang S, Oganov A R and Cheng L 2018 First-principles study of thermoelectric properties of Mg 2 Si–Mg 2 Pb semiconductor materials *RSC Adv.* **8** 17168–75
[56] Kajitani T, Kubouchi M, Kikuchi S, Hayashi K, Ueno T, Miyazaki Y and Yubuta K 2013 High-performance p-type magnesium silicon thermoelectrics *J. Electron. Mater.* **42** 1855–63
[57] Pulikkotil J, Singh D J, Auluck S, Saravanan M, Misra D, Dhar A and Budhani R 2012 Doping and temperature dependence of thermoelectric properties in Mg 2 (Si, Sn) *Phys. Rev.* B-*Condensed Matter and Materials Physics* **86** 155204
[58] Zhao J, Liu Z, Reid J, Takarabe K, Iida T, Wang B, Yoshiya U and John S T 2015 Thermoelectric and electrical transport properties of Mg 2 Si multi-doped with Sb, Al and Zn *J. Mater. Chem.* A **3** 19774–82
[59] de Boor J, Compere C, Dasgupta T, Stiewe C, Kolb H, Schmitz A and Mueller E 2014 Fabrication parameters for optimized thermoelectric Mg 2 Si *J. Mater. Sci.* **49** 3196–204
[60] Akasaka M, Iida T, Matsumoto A, Yamanaka K, Takanashi Y, Imai T and Hamada N 2008 The thermoelectric properties of bulk crystalline n-and p-type Mg 2 Si prepared by the vertical Bridgman method *J. Appl. Phys.* **104** 013703
[61] Ioannou M, Chrissafis K, Pavlidou E, Gascoin F and Kyratsi T 2013 Solid-state synthesis of Mg2Si via short-duration ball-milling and low-temperature annealing *J. Solid State Chem.* **197** 172–80
[62] Zhou S-C and Bai C-G 2011 Microwave direct synthesis and thermoelectric properties of Mg2Si by solid-state reaction *Transactions of Nonferrous Metals Society of China* **21** 1785–9
[63] Ju J, Fang M, Cai H, Yin K and Yan C 2022 Impact of Cr content on the thermoelectric properties of the Cr/Sb co-doped Mg2. 2- xCrx (Si0. 3Sn0. 7) 0.98 Sb0. 02 compound *Mater. Res. Express* **9** 045504
[64] Cheng K, Bu Z, Tang J, Zhang X, Meng X, Li W and Pei Y 2022 Efficient Mg2Si0. 3Sn0. 7 thermoelectrics demonstrated for recovering heat of about 600 K *Mater. Today Phys.* **28** 100887
[65] Nozariasbmarz A, Agarwal A, Coutant Z A, Hall M J, Liu J, Liu R, Malhotra A, Norouzzadeh P, Oeztuerk M C and Ramesh V P 2017 Thermoelectric silicides: A review *Jpn. J. Appl. Phys.* **56** 05DA04
[66] Liu W, Tan X, Yin K, Liu H, Tang X, Shi J, Zhang Q and Uher C 2012 Convergence of conduction bands as a means of enhancing thermoelectric performance of n-type Mg 2 Si 1 − x Sn x solid solutions *Phys. Rev. Lett.* **108** 166601
[67] Mizoguchi H, Muraba Y, Fredrickson D C, Matsuishi S, Kamiya T and Hosono H 2017 The unique electronic structure of Mg2Si: shaping the conduction bands of semiconductors with multicenter bonding *Angew. Chem. Int. Ed.* **56** 10135–9
[68] Borup K A, De Boor J, Wang H, Drymiotis F, Gascoin F, Shi X, Chen L, Fedorov M I, Müller E and Iversen B B 2015 Measuring thermoelectric transport properties of materials *Energy Environ. Sci.* **8** 423–35

[69] Hu X, Mayson D and Barnett M R 2014 Synthesis of Mg2Si for thermoelectric applications using magnesium alloy and spark plasma sintering *J. Alloys Compd.* **589** 485–90

[70] Kato A, Yagi T and Fukusako N 2009 First-principles studies of intrinsic point defects in magnesium silicide *J. Phys. Condens. Matter* **21** 205801

[71] Zhang Q, Su X, Yan Y, Xie H, Liang T, You Y, Tang X and Uher C 2016 Phase segregation and superior thermoelectric properties of Mg2Si1−x Sb x ($0\leqslant x\leqslant 0.025$) prepared by ultrafast self-propagating high-temperature synthesis *ACS Appl. Mater. Interfaces* **8** 3268–76

[72] Cederkrantz D, Farahi N, Borup K, Iversen B, Nygren M and Palmqvist A 2012 Enhanced thermoelectric properties of Mg2Si by addition of TiO2 nanoparticles *J. Appl. Phys.* **111** 023701

[73] Gurunathan R, Hanus R and Snyder G J 2020 Alloy scattering of phonons *Materials Horizons.* **7** 1452–6

[74] Domenicali C and Otter F 1954 Thermoelectric power and electron scattering in metal alloys *Phys. Rev.* **95** 1134

[75] Sankhla A, Kamila H, Naithani H, Mueller E and de Boor J 2021 On the role of Mg content in Mg2 (Si, Sn): Assessing its impact on electronic transport and estimating the phase width by *in situ* characterization and modelling *Mater. Today Phys.* **21** 100471